VTT Technical Research Centre of Finland

Impact of 15-day energy forecasts on the hydro-thermal scheduling of a future Nordic power system

Rasku, Topi; Miettinen, Jari; Rinne, Erkka; Kiviluoma, Juha

Published in:
Energy

DOI:
10.1016/j.energy.2019.116668

Published: 01/02/2020

Document Version
Early version, also known as pre-print

Impact of 15-day energy forecasts on the hydro-thermal scheduling of a future Nordic power system

Topi Rasku[a,*], Jari Miettinen[b], Erkka Rinne[a], Juha Kiviluoma[a]

[a] *VTT Technical Research Centre of Finland Ltd., P.O. Box 1000, FI-02044 VTT, Espoo, Finland*

[b] *Fortum Corporation, P.O. Box 100, FI-00048 FORTUM, Espoo, Finland*

Abstract

One of the most promising ways of de-carbonising the energy sector is through increasing the amounts of variable renewable energy (VRE) generation in power systems. While the inherent uncertainty of VRE is a challenge, it can be mitigated through improved forecasting and energy system modelling. Typically, stochastic energy system studies have focused on the day-ahead horizon of 36 hours ahead of time, while studies about hydro-thermal scheduling and expansion planning often neglect VRE uncertainty entirely. In this work, the potential benefits of extending the horizon of VRE forecasts on the operation of hydro-dominated power systems was examined using a future Nordic system case study. 15-day ensemble weather forecasts were processed into realistic VRE and demand forecasts up to 348 hours ahead of time, and their impact on power system operations was simulated using stochastic unit commitment and economic dispatch optimisation. While decreases in total yearly operational costs, hydropower spillage and wind power curtailment were observed until forecast horizons up to around 132–156 hours ahead of time, the relative reductions remained rather insignificant at around 0.20–0.35 % for the costs, and 0.10 pp for the spillage and curtailment.

Keywords: Unit commitment, Economic dispatch, Hydro-thermal scheduling, Stochastic programming, Energy forecasting

*Corresponding author

Email address: topi.rasku@vtt.fi (Topi Rasku)

Nomenclature

ED	Economic dispatch
FDIR	Total sky direct solar radiation at surface
MAE	Mean absolute error
MEUR	Million euros
O&M	Operations and maintenance
pp	Percentage point
PV	Photovoltaic
SSRD	Surface solar radiation downwards
TYNDP	Ten Year Network Development Plan
UC	Unit commitment
VRE	Variable renewable energy

1. Introduction

Mitigating climate change is a major driver increasing the amount of variable renewable energy (VRE) in power systems around the globe. Weather dependent VRE resources increase the uncertainty in the power system, affecting both the system operators trying to ensure the balance of generation and load, as well as the electricity market participants trying to decide their optimal bids. Thus, dealing with VRE uncertainty via improved weather forecasting and new energy system modelling approaches has been receiving increasing interest.

Better generation forecasts for VRE have long been valuable in power markets. As a result, there is a considerable amount of literature about the various forecasting methods [1, 2], as well as their role in renewable energy integration [3, 4, 5] and microgrid management [6]. In recent years, the focus of energy forecasting has shifted from deterministic approaches towards probabilistic ones [7], in order to better represent the underlying uncertainty in power systems with significant amounts of VRE generation.

The increasing role of VRE resources has also emphasised stochastic modelling of the power system, over more traditional deterministic modelling approaches [8, 9, 10]. Existing literature has studied the impact of different wind power uncertainty representations on a two-stage stochastic unit commitment (UC) and economic dispatch (ED) problem [11], the energy market value of improving the accuracy of short-term wind power forecasts [12], as well as how the economic and reliability impacts of such forecast improvements depend on the generation mix and energy storage capacity of the simulated power system [13]. Recently, Bakirtzis et al. presented a stochastic unified UC&ED model for short-term power system scheduling with a variable time resolution, and used it to study the benefits of stochastic over deterministic scheduling [14], as well as the optimal scheduling of energy storages under short-term uncertainty [15]. Overall, most of the literature agrees that stochastic UC&ED results in lower costs and more robust solutions compared to deterministic approaches, but cautions that the magnitude of the benefits are dependent on the generation mix and energy storage capacity.

All of the above-mentioned studies have focused on the short-term scheduling within common day-ahead market horizons of up to around 36–48 hours ahead of time, which is reasonable for systems without longer-term energy storage. However, in power systems with such storage, e.g. in the form of large hydropower reservoirs or district heating system scale hot water storage, considering the uncertainty in VRE generation beyond the day-ahead horizon might have an impact on the optimal scheduling of the system. Surprisingly, literature about the impact of using longer wind and solar power forecasts seems to be much harder to find. While optimisation horizons ranging from weeks to months and even years are common in hydro-thermal scheduling and expansion planning [16], the short-term uncertainty associated in VRE production is either not represented adequately for dispatch, or is neglected entirely.

Previous approaches to long-term hydro-thermal scheduling have considered the uncertainty of wind power on the weekly [17, 18] or monthly [19] time scales, but resort to deterministic dispatch within these time scales in order to reduce the computational burden. Some studies have also focused on short-term hydro-thermal scheduling using a robust approach under severe load uncertainty [20], as well as with improved technical modelling of pumped hydro units [21]. However, these studies again focus on optimal scheduling on the day-ahead horizon of only 24 hours. The impact of varying forecast lengths on the operation of power systems has been recently studied by Erichset et al. [22], focusing on the CO_2 emissions of an electricity producer park with long-term energy storage. The tested horizons were chosen to represent possible weather forecast ranges 2–14 days ahead, as well as a hypothetical 30 day forecast and a full 365 day perfect horizon. However, the used UC model was deterministic with perfect foresight for all tested horizons, and the use of the long-term energy storage was determined by simple heuristics instead of it being included the UC optimisation.

This paper aims to study the impact of extended weather forecasts on the operational costs of hydro-dominated power systems by using a Nordic case study with actual ensemble weather forecast data in a rolling stochastic unified UC&ED optimisation model. We hypothesise that by utilising weather forecasts beyond the day-ahead horizon, the operational costs of the power system could be reduced further via improved co-scheduling of VRE and hydropower resources. While only hydropower is featured in the chosen case study, similar benefits could be possible with any form of sufficiently long-term energy storage solutions, and potentially even in power systems with significant amounts of slow response thermal power plants. A previous study by the authors [23] is improved upon by including forecasts for solar generation, as well as electricity and heat demands in addition to wind power forecasts. Furthermore, the impact of the modelled forecast horizon is studied until the full 15-day ahead horizon of the ensemble weather forecast data in a more accurate depiction of the Nordic power system.

Section 2 explains all the data and methods used for constructing the hypothetical future Nordic power system, processing the weather ensemble forecasts, as well as the used stochastic UC model. The results of power system simulations with a number of different forecast horizons and time resolutions are presented in Section 3, and the findings are discussed in Section 4. Finally, main conclusions are drawn and summarised in Section 5.

2. Materials and Methods

In order to study the impact of extended weather forecasts on hydro-thermal scheduling, a hypothetical future Nordic power system was constructed based on existing scenario data, as detailed in Section 2.1. Furthermore, large amounts of weather data were aggregated, converted into energy terms, and calibrated as explained in Section 2.2. Only after all the desired power system and weather data had been properly processed, the impact of the extended VRE forecasts on the operational costs of the power system

Table 1: Installed electricity generation capacities by country and energy source, as well as the yearly electricity and heat demands.

	Installed capacity [GW]								Demand [TWh/a]	
	Solar	Wind	Hydro	Biomass	Nuclear	Coal& Lignite	Gas	Oil	Electricity	Heat
DE	64.0	67.2	5.9	6.9	0.0	36.8	27.0	1.3	559.0	121.6
DK	0.8	6.5	0.0	2.9	0.0	1.5	1.0	0.2	35.7	30.0
EE	0.0	0.5	0.0	0.2	0.0	1.4	0.3	0.0	8.3	6.1
FI	0.0	2.9	3.5	3.3	3.4	1.8	3.2	0.6	83.9	45.8
LT	0.1	0.5	0.1	0.1	1.1	0.0	1.4	0.0	10.2	9.9
LV	0.0	0.3	1.6	0.1	0.0	0.0	1.1	0.0	8.1	6.7
NO	0.0	2.4	41.8	0.0	0.0	0.0	0.6	0.0	135.7	6.8
PL	0.1	10.3	1.0	2.1	0.0	20.7	5.4	0.2	168.3	91.3
SE	0.1	9.0	16.7	3.2	7.0	0.1	3.3	0.5	144.2	51.8

could be simulated. A generic energy network optimisation tool called Backbone [24] was used to set up a rolling stochastic unified UC&ED model for optimising the power system operations, briefly described in Section 2.3.

2.1. Nordic case study

The modelled Nordic power system included the countries around the Baltic sea, with the exceptions of excluding Russia and including Norway, as shown in Figure 1. The European Reference Scenario 2016 [25] results for the year 2030 were used for the country-level power and heat generation capacities, as well as their annual energy demands. The resulting country-wise generation capacities, as well as the yearly electricity and heat demands, are presented in Table 1. Similarly, the total transmission capacities between countries were based on the "NTC 2027 reference grid" in the Ten Year Network Development Plan (TYNDP) 2018 [26]. In order to get a finer depiction of the power system, the e-Highway 2050 project [27] "Large scale RES" scenario for the year 2030 was used as the base for the regional division seen in Figure 1, and the generation and transmission capacities within the countries were distributed accordingly. However, Germany and Poland were still represented by single country-wide regions to reduce the complexity of the model, as they were mostly included to provide a more realistic depiction of electricity trading between the Northern and Central European power systems.

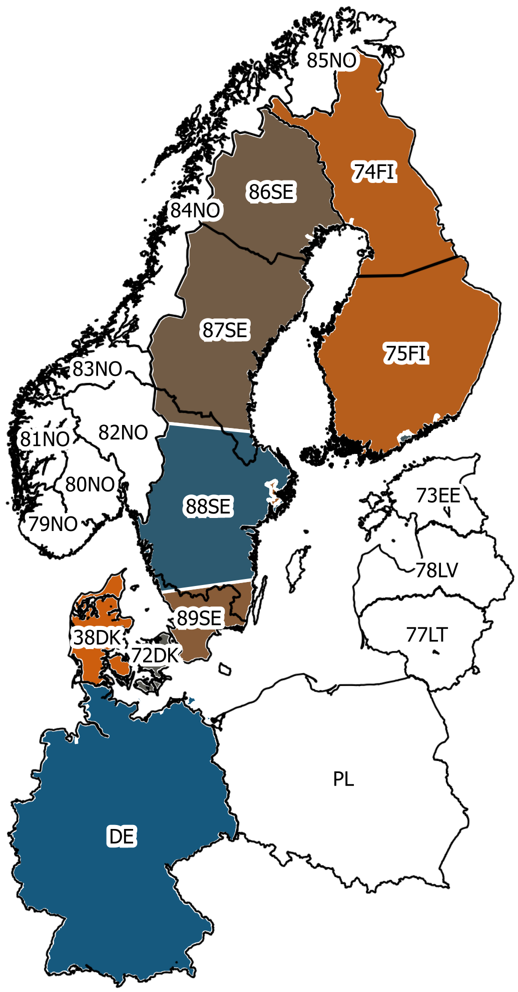

Figure 1: Illustration of the scope of the modelled Nordic power system, and its division into individual regions. The WILMAR project [28] heat areas used for generating the heat demand time series are shown in colour.

Fuel and carbon prices were obtained from the TYNDP 2018 [26] Market Modelling Data “2030 EUCO” scenario, and the CO_2 content of the fuels were based on IPCC guidelines [29]. However, as biomass and biofuel prices weren’t available in the TYNDP 2018 data, estimated future prices from a report by Pöyry Management Consulting Ltd [30] were used for biomass instead. The cost of heating fuels were also increased by applying the minimum excise duty rates as required by the European Union [31].

The technical parameters of the modelled power plants were based on the TYNDP 2018 Market Modelling Data [26], and the required amounts of frequency containment and restoration reserves in the Nordic countries were based on the Nordic System Operation Agreement [32] with the assumption that the new Olkiluoto 3 nuclear power plant becomes the dimensioning fault in the Nordic power system. The reserve requirements in the remaining countries were estimated based on the Continental Europe Operation Handbook [33] parts P1 and A1. Replacement reserves were not included, as they are not used in the Nordic power system.

2.1.1. Electricity and heat demand time series

While the yearly demand for electricity and heat in Table 1 were based on the European Reference Scenario 2016 [25] and e-Highway [27] results, the hourly profiles were generated based on data from ENTSO-E transparency platform [34] for electricity demand, and from the WILMAR project [28] for heat demand. Instead of using the electricity and heat demand time series from the aforementioned sources directly, demand models detailed in Appendix A were used in order to generate demand forecasts based on the weather forecast data discussed in Section 2.2. Unfortunately, the heat demand data was only available for the areas shown in Figure 1, and the heat demand for the remaining regions was estimated using models parameterised with the existing data.

2.1.2. Hydropower inflow time series

Inflow data for hydropower reservoirs and run-of-river hydropower stations was collected from various sources. Weekly inflow time series used for Norway and Sweden were originally simulated using EMPS [35]. The dataset was provided by SINTEF Energi AS (“Hydropower inflow for Norway and Sweden, 1958–2015”, received 24 October 2018). The EMPS areas were mapped to their corresponding regions, and the weekly inflow energies were divided into regulated inflow into reservoirs, and unregulated inflow into

Table 2: Variables used from ERA5 and ENS datasets. SSRD is the surface solar radiation downwards and FDIR is the total sky direct solar radiation at surface (srf). The used model levels are indicated using braces, and roughly correspond to altitudes of 107 m and 170 m.

variable	ERA5	ENS
wind speed [m/s]	100 m, {86, 87}	100 m, {130, 132}
temperature [K]	{srf, 86, 87}	{srf, 130, 132}
pressure [Pa]	{srf}	{srf}
SSRD_{acc} [J/m^2]	{srf}	{srf}
FDIR_{acc} [J/m^2]	{srf}	{srf}
a [Pa]	336.77 {86}	302.48 {130}
	162.04 {87}	122.10 {132}
b [–]	0.97 {86}	0.98 {130}
	0.98 {87}	0.98 {132}

run-of-river hydropower stations. The data was re-sampled to hourly resolution using linear interpolation, and the values were normalised to the annual totals from the European Reference Scenario 2016 [25]. Unfortunately, data for the year 2017, which was used as the weather data in Section 2.2, was not available for the entire modelled area and data from 2012 was used instead. Inflow data for Finland was derived from volumetric inflows from Finnish Environmental Administration [36], and inflows for the rest of the regions were based on data from the WILMAR project [28], again for the year 2012.

2.2. Weather data manipulation

The weather in the simulation was described using ERA5 [37] weather reanalysis data for the year 2017. ERA5 provides a great source of data for energy system modelling, including all spatial and temporal correlations which are paramount for modelling the impacts of VRE generation on the operation of energy systems. As for the weather forecast data, the ENS 15-day ensemble forecasts [38] were used, again for the year 2017. The data was obtained from the surface level and the model levels roughly corresponding to altitudes of 107 m and 170 m, as shown in Table 2 along with the other relevant parameters. Since the model levels are pressure based, the exact altitudes of the model levels vary depending on the surface temperature, and the aforementioned heights were estimated under fixed conditions.

2.2.1. Wind power conversion

In order to calculate the wind power production, the wind speeds must first be estimated for the assumed hub heights. The height h_l at different model levels l could be estimated using the equation [39]

$$h_l = \frac{T_{\mathrm{srf}}}{L}\left[\left(\frac{p_l}{p_{\mathrm{srf}}}\right)^{-\frac{LR}{g}} - 1\right], \tag{1}$$

where T_{srf} is the surface temperature, L is the atmospheric lapse rate of temperature, p_l is the pressure at model level l, p_{srf} is the pressure at the surface, R is specific gas constant and g is the gravitational constant. All the variables in Equation (1) depend on both the coordinates as well as time. In the case of a ENS-data, the variables also depend on the analysis time of the forecast and the ensemble member. The pressure p_l could be calculated by applying model level dependent regression coefficients a and b in Table 2 to equation

$$p_l = a_l + b_l p_{\mathrm{srf}}. \tag{2}$$

The wind speed at altitude h was estimated using wind profile power law

$$w_h = w_r \left(\frac{h}{h_r}\right)^{\alpha}, \tag{3}$$

where w_r and h_r are the reference wind speed and altitude, and α is the profile exponent defined by equation

$$\alpha = \frac{\log(w_{l[\mathrm{low}]}/w_{l[\mathrm{high}]})}{\log(h_{l[\mathrm{low}]}/h_{l[\mathrm{high}]})}, \tag{4}$$

where the low and high subscripts refer to the model level number presented in Table 2. Due to the fluctuating height of the ERA5 and ENS model levels, the reference wind speeds w_r were obtained from fixed reference height $h_r = 100\,\mathrm{m}$ for calculating the wind speeds for the assumed average wind turbine hub height of 140 m.

After the wind speeds are know, the conversion into wind power production $P(w_h)$ is mainly dependent on two components: the wind resource at the the power plant site, and the technological parameters of the used wind turbines. These components can be combined into a power curve equation

$$P(w_h) = P_{\mathrm{pc}}(Sr, c_{\mathrm{p}}, \rho, w_h, w_{\text{cut-off}}, w_{\text{cut-off},\Delta}), \tag{5}$$

where Sr is the specific rating, c_p is the coefficient of performance, ρ is the air density, w_h is the wind speed the at hub height h, $w_\text{cut-off}$ is the cut-off wind speed and $w_{\text{cut-off},\Delta}$ is the associated hysteresis wind speed range for running down the power plant. Equation (5) used a Gaussian filter to smooth the wind speeds according to the methodology in [40] in order to account for the resolution of the weather data and unknown turbulence intensities, and is explained in detail in Appendix B.

2.2.2. Photovoltaic conversion

A method by Pfenninger et al. [41] was used for converting ERA5 and ENS weather data to production capacity factors for solar photovoltaic (PV) panels. Unlike [41], however, the downward component of the direct irradiation (FDIR) and the total diffuse irradiation were used as inputs, and the diffuse irradiation was simply calculated as the difference of surface solar radiation downwards (SSRD) and FDIR. Furthermore, it was assumed that the panels were crystalline silicon with 10 % total system losses, and the panels were rooftop installed with no tracking capability.

The tilt and azimuth angles were again based on [41], with the tilt angle of the panels β following the normal distribution

$$\beta \sim \mathcal{N}(-9.06 + 0.78\phi, (15^\circ)^2), \tag{6}$$

with the mean tilt angle depending on the current latitude ϕ, while the standard deviation was assumed to be 15°. Similarly, the azimuth angle γ followed

$$\gamma \sim \mathcal{N}(180^\circ, (40^\circ)^2), \tag{7}$$

where the mean azimuth angle of the panels was assumed to face south at 180°, and the standard deviation of the azimuth angles was assumed to be 40°.

2.2.3. Forecast calibration

As the realised and forecast and data were obtained from different data sources, the ensemble forecasts had to be calibrated in order to minimise any bias error. In order to reduce the computational burden, the bias was minimised for the modelled regions only, instead of calibrating the forecasts in every coordinate point separately. First, the aggregated capacity weighted regional time series of wind speed and irradiation were calculated for both the ERA5 and the ENS data based on the regional capacities and the assumed power plant locations presented in Figure 2. The locations of most of the wind power plants were based on the wind power plant database [42], including power plants currently under development. However, data from [43] was used for Germany and Denmark for both wind and PV installations. For the rest of the regions, geospatial data for the solar PV installations was not available. Instead, the locations were estimated by clusterising the population density, and using the centre points of the resulting clusters. The weight used for the regional aggregation was the population density of the cluster, multiplied with the cluster area. The population density clustering was also used for weighting the temperature data for the heat and electricity demand models explained in Appendix A.

In order to remove the bias error, the hourly median of the ensemble spread was calculated. Then, the error between the ERA5 data and the ENS data ensemble median ϵ_τ at horizon τ was represented using a generalised additive model

$$\mathbb{E}[\epsilon_\tau] = f_1(\tau) + f_2(H_\tau) + \beta_0, \tag{8}$$

where $f_{1,2}$ are penalised B-splines functions, which all have 20 basis functions, H_τ is the hour of the day at horizon τ, and β_0 is a constant. The pyGAM package [44] was used to solve Equation (8) for the suitable regression functions for correcting the forecast data. Finally, each ensemble member e was corrected using the obtained error

$$Y_{e,\tau}^{\mathrm{corr}} = Y_{e,\tau}^{\mathrm{raw}} - \epsilon_\tau, \tag{9}$$

where Y is the regionally aggregated weather quantity being corrected, namely wind speed, solar irradiation, or temperature. Figure 3 presents the bias and mean absolute error (MAE) of wind speed and SSRD in Germany before and after the bias correction.

Since including the entire set of 50 ensemble forecasts into a large scale power system model was computationally infeasible, the number of the forecasts needed to be reduced. The 20 %, 50 % and 80 % quantiles of the ensemble spread were used to represent the range of uncertainty in the power system model in order to guarantee a certain spread in the forecasts at all times. Figure 4 presents an example of the final wind power capacity factor quantile forecasts in Southern Finland, and the spread of the quantiles can clearly be seen to increase as the forecast horizon increases.

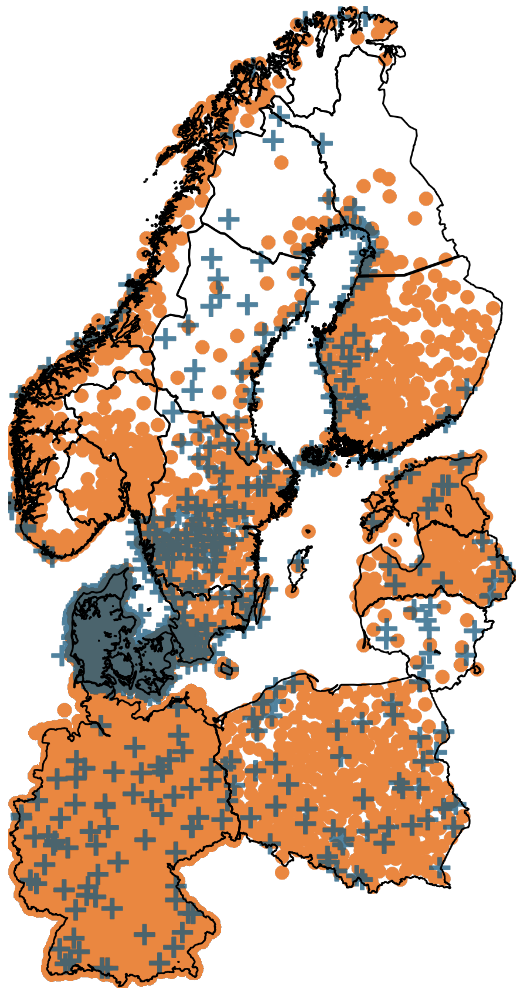

Figure 2: Illustration of the assumed wind and solar power plant locations. Wind power locations are denoted using blue crosses and solar power locations are denoted using orange disks. Geospatial data for solar in Germany and wind in Denmark was abundant, making individual sites indistinguishable in the figure.

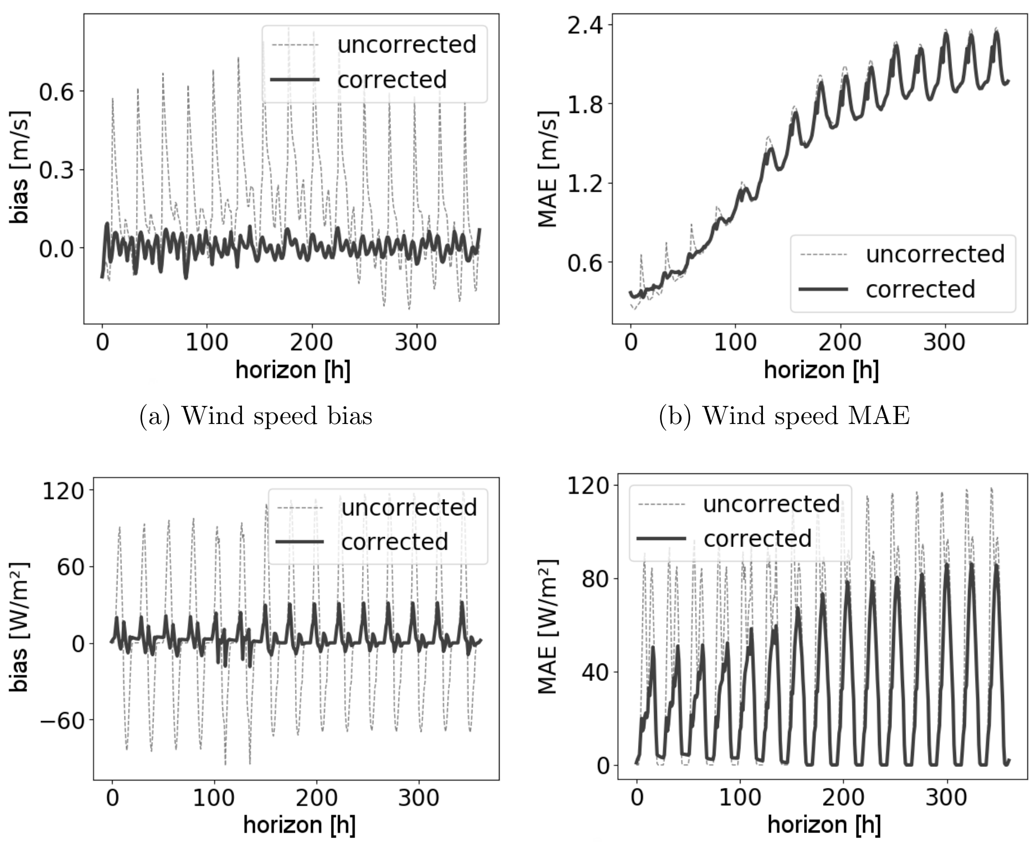

(a) Wind speed bias

(b) Wind speed MAE

(c) SSRD bias

(d) SSRD MAE

Figure 3: SSRD and wind speed bias and MAE on different forecast horizons for Germany before and after the bias correction.

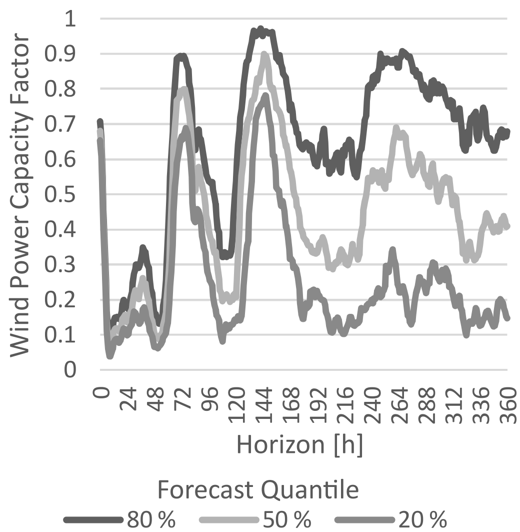

Figure 4: An example of the final wind power capacity factor quantile forecasts for the first two weeks of the simulation in Southern Finland.

2.3. Power system simulation

The rolling stochastic hydro-thermal scheduling of a future Nordic power system was performed using an open source mixed-integer linear programming-based generic energy network optimisation tool called Backbone [24]. The exact version of Backbone used in this work has been tagged as "VaGeResults" in the online repository [45].

The scheduling problem was formulated into a unified UC&ED model reminiscent of [14], but intended for longer modelling horizons required by reservoir hydropower and the extended weather forecasts. Figure 5 presents an illustration of the stochastic structure of a single solve in the rolling optimisation, after which the solution for the first six hours was recorded and the model was solved again starting six hours later in time. The first six hours of each solve represent the operational dispatch of the power system, where the power system has perfect information and dispatches itself accordingly. From the seventh hour up until the desired forecast horizon, the power system has to rely on the uncertain quantile forecast information to commit reserves for the next solve, as well as how to prepare to operate the system in general. The quantile forecasts were updated every 24 hours of model time, as new information became available. In order to reduce the computational burden, the time resolution of the model is progressively decreased

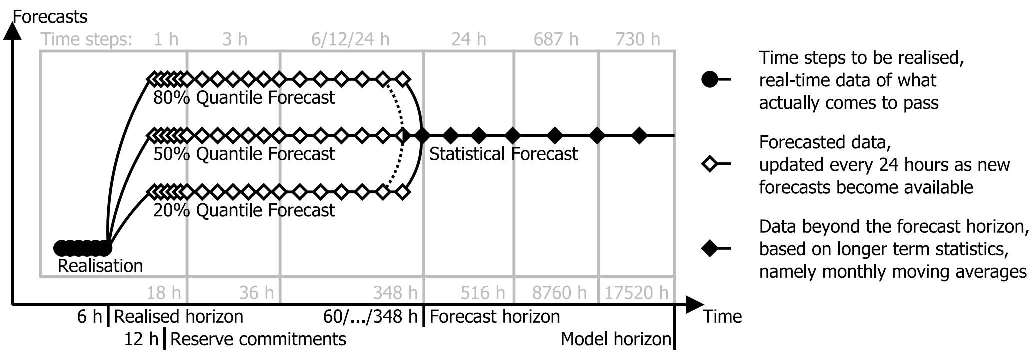

Figure 5: Illustration of the forecast-time structure of a single solve of the unified UC&ED optimisation. The dotted lines demonstrate the changes in the structure and data when the forecast horizon is varied between simulations.

beginning on the nineteenth hour, first to three hour time steps, and then even further as shown in Figure 5. The time resolution from the 36$^{\text{th}}$ hour until the 348$^{\text{th}}$ hour was varied between 6, 12, and 24 hours to determine whether the chosen time resolution has a significant impact on the results. From the forecast horizon until the end of the model horizon at 17,520 hours, the three quantile forecasts converge into a single deterministic forecast using statistical monthly averages.

The impact of extending the VRE forecasts was studied by varying the length of the period when the model used the quantile forecast data before transitioning into the long-term statistical data, as illustrated in Figure 5. The modelled forecast horizons included the 36 hours ahead horizon as a baseline, and each subsequent horizon every 24 hours until the longest modelled forecast horizon of 348 hours ahead. These horizons were chosen to take full advantage of the ENS 15-day ensemble weather forecast data discussed in Section 2.2.

The objective function used in the unified UC&ED problem

$$v^{\text{objective}} = \sum_{f,t} \Bigg[p^{\text{probability}}_{f,t} \Bigg(\sum_{u} \Big[c^{\text{startup\&emission}}_{u} v^{\text{startup}}_{u,f,t} + \Big(c^{\text{O\&M}}_{u} v^{\text{generation}}_{u,f,t} + \sum_{F \in \mathbf{F}_u} \big[c^{\text{fuel\&emission}}_{u,F} v^{\text{fuelUse}}_{u,F,f,t} \big] \Big) \Delta_t \Big] \Bigg) \Bigg] \tag{10}$$

aimed to minimise the *objective* variable representing the total expected operational costs of the power system over all forecasts f and time steps t.

Each forecast-time step was assigned a *probability* parameter, assumed to be 0.6 for the 50 % quantile forecast, 0.2 for both the 80 % and 20 % quantile forecasts, and 1.0 for both the realisation and the long-term statistical forecast. The *startup&emission* cost parameter included all the operational and maintenance, fuel, and emission related costs associated with the unit *startup* variable, while the operations and maintenance (*O&M*) and *fuel&emission* cost parameters were handled separately along with the unit energy *generation* and *fuelUse* variables respectively. As the *generation* and *fuelUse* variables represent average power during time step t, they were multiplied with the length of the time step Δ_t to obtain the total costs over the time step. The presented objective function in Equation (10) has been simplified from its full formulation in [24] for clarity by omitting grid and node dimensions, as well as all unused terms. In the model, nodes represent points for calculating energy balance, while grids are used to group nodes with the same energy carrier together.

The hydropower reservoirs were modelled as simple energy equivalent aggregate reservoirs, one for each of the modelled power system region with reservoir hydropower. The dynamics of the reservoirs were governed by the generic energy balance equation

$$\begin{aligned} v^{state}_{n,f,t} - v^{\text{state}}_{n,f,t-1} = &\Big(\sum_{n' \in \mathbf{N}_n} \big[(1 - p^{\text{transferLoss}}_{n',n}) v^{\text{transfer}}_{n',n,f,t} - v^{\text{transfer}}_{n,n',f,t} \big] \\ &+ \sum_{u \in \mathbf{U}_n} \big[\pm v^{\text{generation}}_{n,u,f,t} \big] - v^{\text{spill}}_{n,f,t} \pm \tau^{\text{influx}}_{n,f,t} \Big) \Delta_t \\ \forall \{n, f, t\}, & \end{aligned} \tag{11}$$

where the *state* variables were used for keeping track of the amount of energy stored in the reservoir nodes, and water inflow was represented using the *influx* time series. The reservoir nodes were not connected to any other nodes via *transfer* variables, but were able to spill excess energy using the *spill* variable. The *generation* variable and the *influx* time series are included in Equation (11) using a $\pm$ for clarity, as they can be both positive and negative depending on the desired application. The set $\mathbf{N}_n$ contains all nodes n' connected to node n via energy *transfer* variables, and the set $\mathbf{U}_n$ contains all the units u that either output energy to node n, or draw energy from it as input using the *generation* variable. The *transferLoss* parameter was simply assumed to be 0.01 for all transmission lines, regardless of their capacity or length. The presented Equation (11) has been simplified from its full formulation in [24] by omitting the grid dimension, as well as all unused terms. Run-of-river hydropower was aggregated similarly to the reservoir hydropower, except that no *state* variables were used in Equation (11) as run-of-river power plants were assumed to lack significant amounts of storage.

Equation (11) was also used for ensuring the balance of the power and heat systems by removing the *state* and *spill* variables, essentially reducing the equation to a power balance constrain instead. The *transfer* variables represented power transmission in the power grid, and the *influx* time series represented the power and heat demands. Neither power nor heat nodes were allowed to use the *spill* variable to get rid of excess energy in the system.

Further constraints were implemented to restraint power transmission capacities, reserve balance and provision, as well as unit conversion efficiencies and online dynamics. These constraints are not presented here, however, as they are not crucial for understanding this study. Instead, interested readers are instead encouraged to take a look at the full model methodology presented in [24].

3. Results

The impact of extended weather forecasts on the operation of the modelled Nordic power system was studied by performing full year rolling stochastic unified UC&ED simulations using different forecast horizons. The time resolution between the 36$^{\text{th}}$ hour and the 348$^{\text{th}}$ hour of each solve was reduced to improve computational performance, and the power system simulations were carried out using time resolutions of 6 hours, 12 hours, and 24 hours. The total computational time of the simulations was 27–77 hours when using the 6-hour time resolution depending on the modelled forecast horizon length, and 18–24 hours using a 24-hour time resolution on a Intel® Xeon® CPU E5-2620 @ 2.00 GHz using GAMS 24.0.2. The simulations with the 12-hour time resolution took around 17–30 hours depending on the modelled forecast horizon, but were run on Intel® Xeon® CPU W3690 @ 3.47 GHz using GAMS 24.1.3 instead, so the computational times are not directly comparable.

Figure 6 presents the total yearly operational costs of the simulated power system as a function of the modelled forecast horizon, as well as the different cost components, with all the simulated forecast time resolutions. As hypothesised, the total operational costs of the power system could be seen to decrease as the modelled forecast horizon increases, but only until around

132–156 hours ahead. Interestingly, the total fuel and emission costs of the power system increased at forecast horizons above 132 hours, while the O&M and startup costs of the units maintained a slight decreasing trend. Overall, the total operational cost savings achieved by increasing the forecast horizon remain rather modest, only around 0.20–0.35 % (58–99 MEUR) per year. The total yearly CO_2 emissions behaved similarly to the total fuel and emission costs presented in 6b, decreasing by around 0.33–0.94 % (0.90–2.54 $MtCO_2$).

As expected, the better accuracy of smaller time resolutions was seen to result in the lowest total yearly operational costs for most of the modelled forecast horizons. The differences in the total costs of the 12-hour and 24-hour time resolutions compared to the 6-hour resolution were relatively modest, between 0.00–0.05 % (−2–14 MEUR) and 0.04–0.10 % (11–28 MEUR) respectively. Even though the absolute values differ slightly between the used time resolutions, the overall trend in the different costs for the different forecast horizons remained quite similar. Interestingly, however, while the 6-hour time resolution resulted in the lowest total O&M and startup costs of all the tested resolutions, its fuel and emission costs were noticeably higher than those of the 12-hour and 24-hour resolutions.

The total electricity generation by source over the modelled year is presented in Figure 7a, with the changes compared to the 36 hours ahead forecast horizon highlighted in Figure 7b. The use of biomass could be seen to increase noticeably, by around 13–23 % (5–8 TWh), until a forecast horizon of 156 hours ahead. The increasing biomass generation replaced both coal and gas generation, decreasing them by around 5–8 % (3–6 TWh) and 1–4 % (2–6 TWh) respectively. Interestingly, while gas generation was observed to decrease until the longest modelled horizon of 348 hours ahead of time, coal generation reached its minimum at the 156 hour horizon, after which it was observed to slowly increase again.

Figure 8 presents the share of total curtailed wind power production, as well as total spilled hydropower relative to the yearly inflows, as a function of the modelled forecast horizon. Both the curtailment of wind power and hydropower spillage could be seen to decrease as the modelled forecast horizon increased. PV generation was not curtailed in any of the simulations due to it having the cheapest operational costs of all the modelled generation technologies. However, the wind and hydropower resources were already almost fully utilised before extending the forecast horizon, so the reductions in curtailment and spill remained modest around 0.10 pp. Unlike with the total yearly operational costs, no clear differences in wind power curtailment and

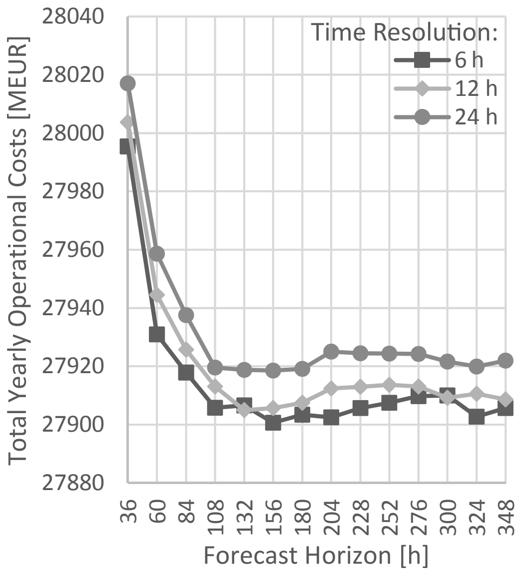

(a) Total system costs

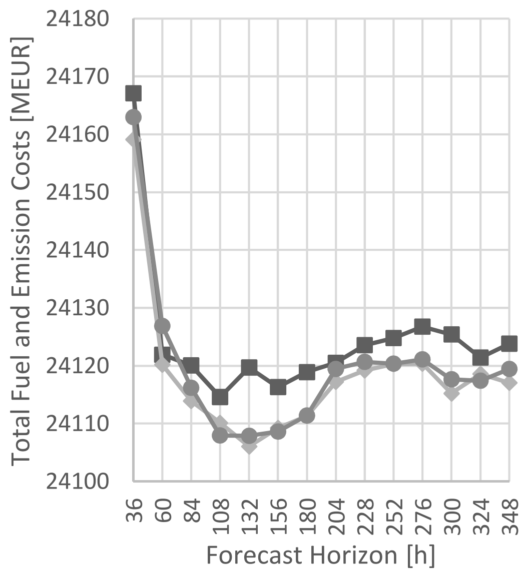

(b) Total fuel & emission costs

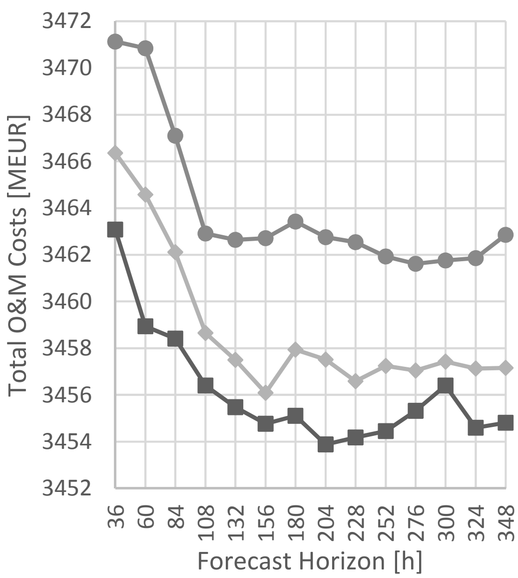

(c) Total O&M costs

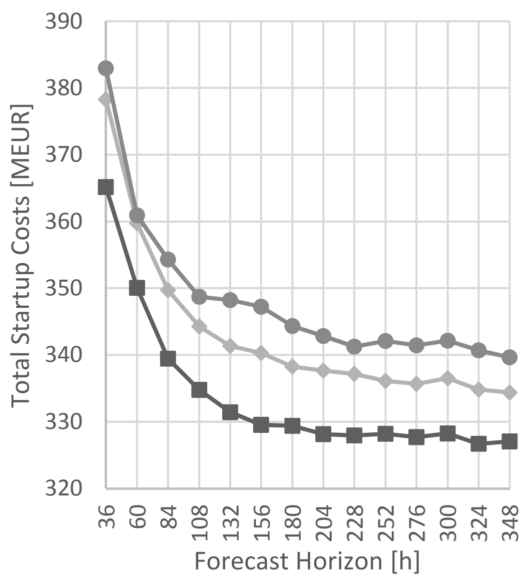

(d) Total startup costs

Figure 6: Total yearly operational costs (a) of the power system as a function of forecast horizon with multiple time resolutions, as well as a breakdown of the individual cost components. The fuel and emission costs (b) can be seen to account for the majority of the total costs, while the O&M (c) and startup (d) costs play less significant roles.

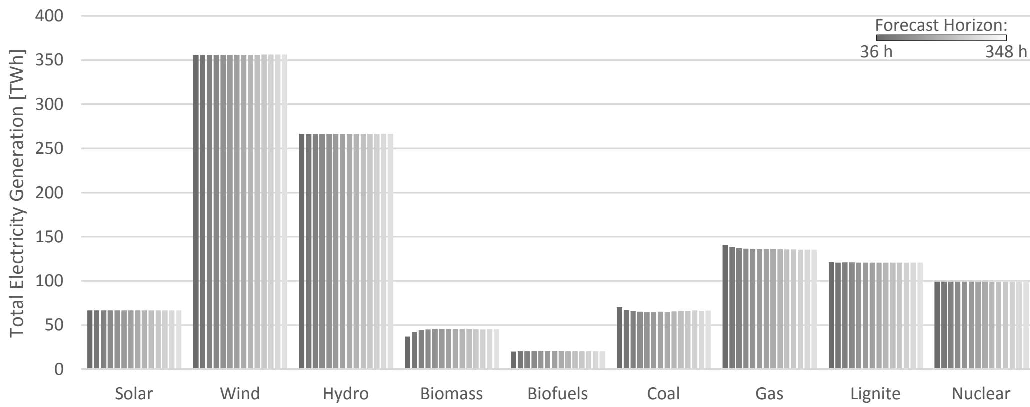

(a) Total yearly electricity generation by source

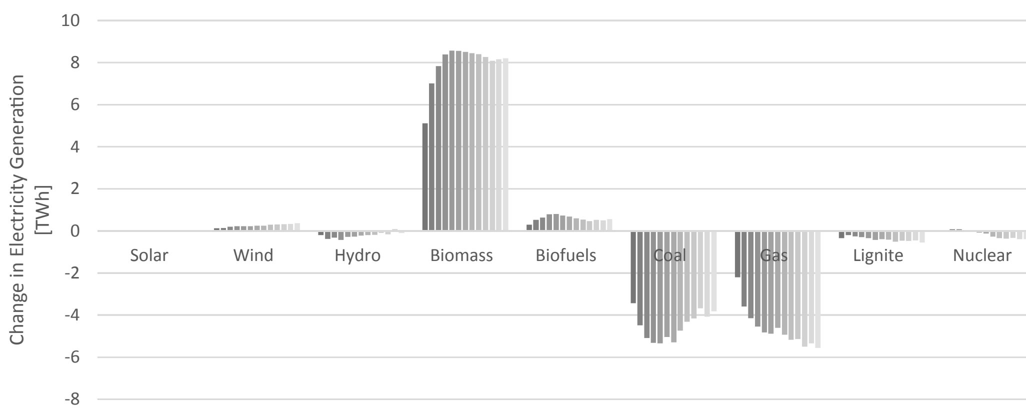

(b) Change compared to the 36 hour ahead forecast horizon

Figure 7: Total electricity generation by source for different modelled forecast horizons with 6-hour time resolution (a), and its changes compared to the 36 hours ahead forecast horizon (b). Darker shades of grey indicate a shorter forecast horizon. Oil-fired generation has been omitted due to negligible total generation levels below 1 GWh with all modelled forecast horizons.

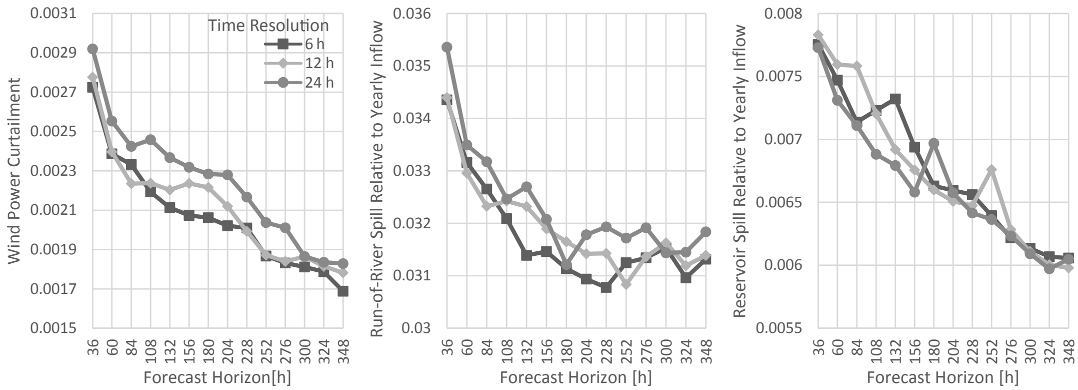

(a) Wind curtailment (b) Run-of-river spill (c) Reservoir spill

Figure 8: Share of total curtailed wind power production (a), as well as the total spilled run-of-river (b) and reservoir hydropower (c) relative to their yearly inflows as a function of forecast horizon with multiple time resolutions.

hydropower spillage between the different time resolutions could be seen.

Figure 9 presents the total energy in all the hydropower reservoirs over the simulations with different forecast horizons. The extended weather forecasts only have a barely noticeable impact on the total use of hydropower reservoirs, although the relative differences in reservoir energy content between the horizons could be up to around 13–16 % in spring, when the reservoir levels were at their lowest. For individual reservoirs and especially for pumped hydro storage plants, the differences between the simulations were higher, but didn't seem to impact the overall use of reservoir energy.

4. Discussion

While the total yearly operational costs of the modelled power system could be seen to decrease when increasing the forecast horizon beyond 36 hours typical of day-ahead simulations, the benefits rather quickly stagnated around forecast horizons of 132–156 hours. Most of the observed cost decreases at forecast horizons between 36–132 hours due to the rapid decline in fuel and emission costs shown in Figure 6b, driven by cheaper biomass based generation replacing coal and gas based generation as seen from Figure 7b. With longer forecast horizons of 132–348 hours, however, the total fuel and emission costs could be seen to slowly increase, along with coal based generation.

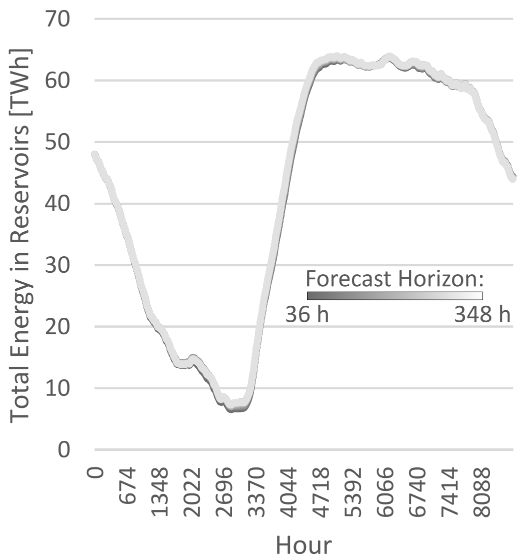

Figure 9: Total energy in all the hydropower reservoirs over the simulations with different forecast horizons using the 6-hour time resolution. Darker shades of grey indicate a shorter forecast horizon.

The observed increase in fuel and emission costs could potentially be explained by the increasing spread of the quantile forecasts at longer horizons, as seen in the example forecasts presented in Figure 4. With sufficiently large forecast uncertainty at the end of the forecast horizon, the expected operational cost minimisation could favour excessively robust solutions, but determining the exact mechanism through which the costs were increased is challenging. While the model was observed keeping increasing amounts of idle capacity online on longer forecast horizons, slightly decreasing the average efficiency of the generation fleet, this effect alone couldn't fully explain the observed increase in fuel and emission costs.

Another possible way for the model to brace itself for the perceived uncertainty could have been to use reservoir hydropower more sparingly. This was considered unlikely, however, as there were no significant differences observed in total stored reservoir energy as the forecast horizon was increased, as shown in Figure 9, nor in the total hydropower generation shown in Figure 7b. Based on these results, it would indeed seem that accounting for short-term VRE variability in long-term hydro-thermal expansion planning [17, 19, 18] wouldn't result in significant differences on the long-term scheduling. However, in order to ascertain this, the long-term stochasticity in yearly hydropower inflows would have to be properly accounted for in addition to the short-term VRE variability. Furthermore, increasing the forecast horizon length was observed to affect the operational strategies of differently sized reservoirs individually. Even though the differences evened out when comparing the total reservoir energy of the system in the simulations, assessing the implications of extended forecast horizons on energy storages of different sizes could be a topic for further research.

All in all, the results show that there was some additional value in extending the forecast horizon beyond the day-ahead horizon of 24–36 hours typically used in existing literature on stochastic UC&ED [11, 12, 13, 14, 21, 15, 20]. However, no clear savings were observed beyond forecast horizons of around 132–156 hours ahead of time. It is also worth noting that since most of the observed system cost savings were achieved via biomass replacing coal and gas, the results are potentially quite sensitive to the fuel and carbon price assumptions. Furthermore, while the observed decrease in CO_2 emissions was not quite as negligible as the one in the study by Erichsen et al. [22], it still remained relatively small compared to the total yearly emissions of the modelled Nordic power system.

Increasing the modelled forecast horizon was observed to reduce both the curtailment of wind power, as well as the spillage of reservoir and run-of-river hydropower, as seen in Figure 8. However, the modelled power system was large and flexible enough to be able to utilise most of these resources already at the shortest modelled forecast horizon of 36 hours, making the reductions in wind power curtailment and hydropower spillage largely negligible. The impact of extended weather forecasts in decreasing wind power curtailment and hydropower spillage could be more meaningful in a different case study with a significant reliance on VRE generation, or in an isolated system. Such case studies could be an interesting line of possible future work, along with determining if improving the accuracy of the ensemble forecasts past the 132 hour mark would result in meaningful improvements for the optimal scheduling of the power system.

Somewhat surprisingly, the overall trends in both the total yearly operational costs as well as the wind power curtailment and hydropower spillage were found to be rather consistent across the 6-hour, 12-hour, and 24-hour time resolutions. While each time resolution had noticeably different cost levels, the costs behaved in a similar manner for all of the time resolutions when the forecast horizon was increased. Since the simulations with the coarser time resolutions didn't affect the trends in the results, it would seem that adjusting the time resolution could be useful e.g. for acquiring preliminary results in less time.

5. Conclusions

This work aimed to study the potential benefits of using extended weather forecasts for improving the hydro-thermal scheduling of hydro-dominated power systems. While the total yearly operational costs were seen to decrease as the modelled forecast horizon was increased beyond the typical day-ahead horizon of 36 hours until around 132–156 hours, the relative costs savings remained relatively small at around 0.20–0.35 % per year. Further cost reductions were not observed with forecast horizons between 156–348 hours, but further research is required to ascertain whether this is due to the increasing spread of the underlying ensemble weather forecasts, or due to the properties of the modelled power system.

Similarly, only slight decreases of around 0.10 pp in wind power curtailment and hydropower spillage were observed. However, the modelled Nordic power system was already able to utilise its wind and hydropower resources almost fully at the 36 hours ahead forecast horizon. Further research is required to see if extended weather forecasts could reduce wind power and hydropower spill in more isolated power systems, or in power systems with significantly higher dependance on VRE resources.

Acknowledgements

This study was supported by the Academy of Finland project “Improving the value of variable and uncertain power generation in energy systems (VaGe)” (grant number 284973), which is part of the New Energy programme; as well as by the Strategic Research Council at the Academy of Finland, project “Transition to a resource efficient and climate neutral electricity system (EL-TRAN)” (grant number 314319).

The hydropower inflow time series for Norway and Sweden were kindly provided by Linn Emelie Schäffer at SINTEF Energy AS.

Appendix A. Demand models

Generally, both electricity and heat demand on large enough scales are dependent on ambient temperatures due to e.g. direct electrical heating.

Additionally, both demands are also dependent on daily cycles due to societal patterns, such as business days and industrial processes. In this work, the electricity demand D_t^{elec} at time t was modelled using a generalised additive model

$$\mathbb{E}[D_t^{\mathrm{elec}}] = f_1(T_t) + f_2(H_t) + f_3(B_t) + f_4(m_t) + \beta_0, \tag{A.1}$$

where T_t is the ambient temperature, H_t is the hour of the day, B_t is a boolean for business days, m_t is the month, and β_0 is a constant. The penalized B-spline functions from $f_{1,\ldots,4}$ were estimated using pyGAM [44]. Similarly, the heat demand D_t^{heat} followed

$$\mathbb{E}[D_t^{\mathrm{heat}}] = f_1(T_{t,\mathrm{MA24}}) + f_2(T_t) + f_3(H_t) + f_4(W_t) + f_5(m_t) + \beta_0, \tag{A.2}$$

where $T_{t,\mathrm{MA24}}$ is the 24-hour moving average of the ambient temperature T_t, and W_t is the weekday. Tables A.3 and A.4 present the bias, MAE, and standard deviation of the errors in the electricity and heat demand models respectively.

Table A.3: Bias, MAE and standard deviation (sd) of errors of the electricity demand model in Equation (A.1). The values are given as per units from the peak demand.

country	bias/10^{-12}	MAE	sd
DE	1.005	0.041	0.055
DK	0.660	0.025	0.032
EE	0.934	0.030	0.039
FI	1.028	0.020	0.026
LT	1.018	0.033	0.043
LV	0.970	0.035	0.045
NO	0.857	0.017	0.024
PL	1.051	0.036	0.052
SE	0.912	0.023	0.030

Appendix B. Power curve model

The per unit wind power conversion from wind speed to power can be expressed as

$$P_{\mathrm{pu}}(w) = \frac{1}{2Sr}\rho w^3 c_{\mathrm{p}}, \tag{B.1}$$

Table A.4: Bias, MAE and standard deviation (sd) of errors of the heat demand model in Equation (A.2). The values are given as per units from the peak demand.

heat area	bias/10^{-12}	MAE	sd
DK_W_Rural	0.256	0.042	0.056
SE_M_Urban	0.219	0.060	0.076
SE_M_Rural	0.099	0.061	0.076
FI_R_Rural	0.302	0.050	0.066
SE_N_Rural	0.206	0.062	0.078
DE_All	0.206	0.025	0.033
DK_E_Urban	0.205	0.039	0.054
SE_S_Rural	0.188	0.061	0.077
FI_R_Urban	0.276	0.057	0.071

where Sr is specific rating, which is the rated power divided by the swept area of the rotor $Sr = P_{\max} \ / \ A$, ρ is the density of the air, w is the wind speed at the desired height and c_{p} is the coefficient of the performance. An important parameter that can be derived from Equation (B.1) is the rated wind speed

$$w_{\mathrm{rated}} = \sqrt[3]{\frac{2Sr}{\rho c_{\mathrm{p}}}}, \tag{B.2}$$

showing that by lowering the specific rating or by increasing c_{p}, the rated wind speed can be lowered. As the wind speed increases, the wind speed reaches a cut-off wind speed, $w_{\text{cut-off}}$ which after the power production is run down. The power curve model in this work assumed that the power production was run down linearly from $P_{\mathrm{pu}}(w_{\text{cut-off}} - w_{\text{cut-off},\Delta}) = 1$ to $P_{\mathrm{pu}} w_{\text{cut-off}} + w_{\text{cut-off},\Delta}) = 0$. Furthermore, $w_{\text{cut-off}}$ was assumed to be equal to 22 m/s and the hysteresis parameter $w_{\text{cut-off},\Delta}$ was assumed to be equal to 1 m/s.

However, Equation (B.1) has two major drawbacks: first, the equation assumes that the wind resource has no turbulence, and second, the ERA5 wind speed data has 0.25° spatial resolution and the value must correspond to the total wind power production over the wind power plants in the 0.25° grid. Following the methodology in [40], a Gaussian filter was used to smooth the power curve in (B.1) according to

$$P(w, \delta_w, \sigma) = \int_{v=0}^{\infty} P_{\mathrm{pu}}(v + \delta_w) f(v, w, \sigma) dv, \tag{B.3}$$

where $f(v, w, \sigma)$ is the probability density function of a normal distribution with mean w and standard deviation σ, and δ_w is a correction constant for the wind speed. It was assumed that the standard deviation follows the equation $\sigma = Iw$, where I is the turbulence intensity. In practice, the integral in Equation (B.3) was discretised and the upper limit for the sum was $50\,\mathrm{m/s}$.

The zero turbulence power curve $P_{\mathrm{pu}}(w)$ and it's c_{p} can be calculated using a method presented in [46], which is based on iterating Equation (B.3) and assumes that the zero turbulence power curve has a constant c_{p} between cut-in and rated wind speed. In theory, the state-of-the-art variable speed wind power plants can operate with optimal c_{p} by operating the turbine at the optimal tip-speed ratio by regulating the pitch angle. In this work, zero turbulence curves were solved for five different wind power technologies used in ten different wind power plants in Finland using sales power curves, which are standardised using IEC standard [46] $\rho = 1.225\,\mathrm{kg/m^3}$ and turbulence intensity $I = 0.1w$. These zero turbulence power curves were assumed to be reasonable for the other modelled countries as well, and were used for all of the modelled power system regions.

Additionally, since the turbulence intensity in the ERA5 data is unknown, the standard deviation in the Gaussian filter was estimated as

$$\sigma(a, b) = a + bw_{\mathrm{ERA}}, \tag{B.4}$$

following the methodology in [47]. The values for the parameters a, b and δ_w were determined by minimising the weighted absolute error over time t, using weights $u(w_t)$ from the wind speed distribution probability density function and using ERA5 wind speeds from 100 meters

$$\min_{\delta_w, a, b} \sum_{t=1}^{8760} u(w_{\mathrm{ERA},t}) \left| \Phi_t - P(w_{\mathrm{ERA},t}, \delta_w, a, b) \right|, \tag{B.5}$$

resulting in $a = 0.35$ and $b = 0.075$, where Φ_t was the measured wind power production from the Finnish wind power plant. The wind speed correction term δ_w varied from site to site, and it's main purpose was to correct bias between the ERA5 and actual wind speeds, such that the parameters a and b from different sites and wind power technologies were comparable. This all results into the power curve model

$$P(w) = P_{\mathrm{pc}}(Sr, c_{\mathrm{p}}, \rho, w, w_{\text{cut-off}}, w_{\text{cut-off},\Delta}). \tag{B.6}$$

References

[1] M. Lei, L. Shiyan, J. Chuanwen, L. Hongling, Z. Yan, A review on the forecasting of wind speed and generated power, Renewable and Sustainable Energy Reviews 13 (4) (2009) 915–920. doi:10.1016/j.rser.2008.02.002.

[2] J. Antonanzas, N. Osorio, R. Escobar, R. Urraca, F. J. Martinez-de pison, F. Antonanzas-torres, Review of photovoltaic power forecasting, Solar Energy 136 (2016) 78–111. doi:10.1016/j.solener.2016.06.069. Available at: http://dx.doi.org/10.1016/j.solener.2016.06.069

[3] E. B. Ssekulima, M. B. Anwar, A. Al Hinai, M. S. El Moursi, Wind speed and solar irradiance forecasting techniques for enhanced renewable energy integration with the grid: a review, IET Renewable Power Generation 10 (7) (2016) 885–989. doi:10.1049/iet-rpg.2015.0477.

[4] G. Notton, M. L. Nivet, C. Voyant, C. Paoli, C. Darras, F. Motte, A. Fouilloy, Intermittent and stochastic character of renewable energy sources: Consequences, cost of intermittence and benefit of forecasting, Renewable and Sustainable Energy Reviews 87 (December 2016) (2018) 96–105. doi:10.1016/j.rser.2018.02.007. Available at: https://doi.org/10.1016/j.rser.2018.02.007

[5] A. Ahmed, M. Khalid, A review on the selected applications of forecasting models in renewable power systems, Renewable and Sustainable Energy Reviews 100 (September 2018) (2019) 9–21. doi:10.1016/j.rser.2018.09.046. Available at: https://doi.org/10.1016/j.rser.2018.09.046

[6] A. Agüera-Pérez, J. C. Palomares-Salas, J. J. González de la Rosa, O. Florencias-Oliveros, Weather forecasts for microgrid energy management: Review, discussion and recommendations, Applied Energy 228 (June) (2018) 265–278. doi:10.1016/j.apenergy.2018.06.087. Available at: https://doi.org/10.1016/j.apenergy.2018.06.087

[7] Y. Ren, P. N. Suganthan, N. Srikanth, Ensemble methods for wind and solar power forecasting - A state-of-the-art review, Renewable and Sustainable Energy Reviews 50 (2015) 82–91. doi:10.1016/j.rser.2015.04.081. Available at: http://dx.doi.org/10.1016/j.rser.2015.04.081

[8] Q. P. Zheng, J. Wang, A. L. Liu, Stochastic Optimization for Unit Commitment - A Review, IEEE Transactions on Power Systems 30 (4) (2015) 1913–1924. doi:10.1109/TPWRS.2014.2355204.

[9] W. van Ackooij, I. Danti Lopez, A. Frangioni, F. Lacalandra, M. Tahanan, Large-scale unit commitment under uncertainty: an updated literature survey, Annals of Operations Research 271 (1) (2018) 11–85. doi:10.1007/s10479-018-3003-z.
Available at: https://doi.org/10.1007/s10479-018-3003-z

[10] M. Håberg, Fundamentals and recent developments in stochastic unit commitment, International Journal of Electrical Power and Energy Systems 109 (February) (2019) 38–48. doi:10.1016/j.ijepes.2019.01.037.
Available at: https://doi.org/10.1016/j.ijepes.2019.01.037

[11] J. Wang, A. Botterud, R. Bessa, H. Keko, L. Carvalho, D. Issicaba, J. Sumaili, V. Miranda, Wind power forecasting uncertainty and unit commitment, Applied Energy 88 (11) (2011) 4014–4023. doi:10.1016/j.apenergy.2011.04.011.
Available at: http://dx.doi.org/10.1016/j.apenergy.2011.04.011

[12] E. V. Mc Garrigle, P. G. Leahy, Quantifying the value of improved wind energy forecasts in a pool-based electricity market, Renewable Energy 80 (2015) 517–524. doi:10.1016/j.renene.2015.02.023.
Available at: http://dx.doi.org/10.1016/j.renene.2015.02.023

[13] Q. Wang, C. B. Martinez-Anido, H. Wu, A. R. Florita, B. M. Hodge, Quantifying the Economic and Grid Reliability Impacts of Improved Wind Power Forecasting, IEEE Transactions on Sustainable Energy 7 (4) (2016) 1525–1537. doi:10.1109/TSTE.2016.2560628.

[14] E. A. Bakirtzis, P. N. Biskas, Multiple Time Resolution Stochastic Scheduling for Systems With High Renewable Penetration, IEEE Transactions on Power Systems 32 (2) (2017) 1030–1040. doi:10.1109/TPWRS.2016.2574645.

[15] E. A. Bakirtzis, C. K. Simoglou, P. N. Biskas, A. G. Bakirtzis, Storage management by rolling stochastic unit commitment for high renewable energy penetration, Electric Power Systems Research 158 (2018) 240–249. doi:10.1016/j.epsr.2017.12.025.
Available at: http://dx.doi.org/10.1016/j.epsr.2017.12.025

[16] A. R. De Queiroz, Stochastic hydro-thermal scheduling optimization: An overview, Renewable and Sustainable Energy Reviews 62 (2016) 382–395. doi:10.1016/j.rser.2016.04.065.
Available at: http://dx.doi.org/10.1016/j.rser.2016.04.065

[17] A. Helseth, A. Gjelsvik, B. Mo, Ú. Linnet, A model for optimal scheduling of hydro thermal systems including pumped-storage and wind power, IET Generation, Transmission & Distribution 7 (12) (2013) 1426–1434. doi:10.1049/iet-gtd.2012.0639.

[18] A. Helseth, B. Mo, A. Lote Henden, G. Warland, Detailed long-term hydro-thermal scheduling for expansion planning in the Nordic power system, IET Generation, Transmission & Distribution 12 (2) (2017) 441–447. doi:10.1049/iet-gtd.2017.0903.

[19] S. R. Silva, A. R. De Queiroz, L. M. M. Lima, J. W. M. Lima, Effects of wind penetration in the scheduling of a hydro-dominant power system, IEEE Power and Energy Society General Meeting 2014-Octob (October). doi:10.1109/PESGM.2014.6939121.

[20] S. E. Razavi, A. Esmaeel Nezhad, H. Mavalizadeh, F. Raeisi, A. Ahmadi, Robust hydrothermal unit commitment: A mixed-integer linear framework, Energy 165 (2018) 593–602. doi:10.1016/j.energy.2018.09.199.
Available at: https://doi.org/10.1016/j.energy.2018.09.199

[21] G. E. Alvarez, M. G. Marcovecchio, P. A. Aguirre, Security-Constrained Unit Commitment Problem including thermal and pumped storage units: An MILP formulation by the application of linear approximations techniques, Electric Power Systems Research 154 (2018) 67–74. doi:10.1016/j.epsr.2017.07.027.
Available at: https://doi.org/10.1016/j.epsr.2017.07.027

[22] G. Erichsen, T. Zimmermann, A. Kather, Effect of Different Interval Lengths in a Rolling Horizon MILP Unit Commitment with Non-Linear Control Model for a Small Energy System, Energies 12 (6) (2019) 1003. doi:10.3390/en12061003.
Available at: https://www.mdpi.com/1996-1073/12/6/1003

[23] J. J. Miettinen, J. Ikaheimo, T. Rasku, H. Holttinen, J. Kiviluoma, Impact of longer stochastic forecast horizon on the operational cost of

a power system, in: International Conference on the European Energy Market, EEM, IEEE, Lodz, 2018. doi:10.1109/EEM.2018.8469219.

[24] N. Helistö, J. Kiviluoma, J. Ikäheimo, T. Rasku, E. Rinne, C. O'Dwyer, R. Li, D. Flynn, Backbone – an adaptable energy systems modelling framework, to be submitted (2019).
Available at: https://cris.vtt.fi/en/publications/backbone-an-adaptable-energy-systems-modelling-framework

[25] Directorate-General for Energy, Energy Modelling - EU Reference Scenario 2016 (2016).
Available at: https://data.europa.eu/euodp/data/dataset/energy-modelling

[26] European Network of Transmission System Operators for Electricity (ENTSO-E), TYNDP 2018 (2018).
Available at: https://tyndp.entsoe.eu/tyndp2018/

[27] e Highway 2050 consortium, e-Highway2050 Results (2013).
Available at: http://www.e-highway2050.eu/results/

[28] P. Meibom, R. Barth, I. Norheim, H. Ravn, P. Sørensen, Wind Power Integration in a Liberalised Electricity Market - WILMAR Final Technical Report, Tech. rep., Risoe National Laboratory, Roskilde (2006).
Available at: http://www.wilmar.risoe.dk/Deliverables/WilmarFinalTechnicalReportPublic.pdf

[29] D. R. Gómez, J. D. Watterson, B. B. Americanohia, C. Ha, G. Marland, E. Matsika, L. N. Namayanga, B. Osman-Elasha, J. D. K. Saka, K. Treanton, Stationary Combustion, in: S. Eggleston, L. Buendia, K. Miwa, T. Ngara, K. Tanabe (Eds.), 2006 IPCC Guidelines for National Greenhouse Gas Inventories, Institute for Global Environmental Strategies (IGES), Hayama, Kanagawa, 2006, Ch. 2, p. 47. arXiv:arXiv:1011.1669v3, doi:10.1016/S0166-526X(06)47021-5.
Available at: http://www.ipcc-nggip.iges.or.jp/public/2006gl/pdf/2_Volume2/V2_2_Ch2_Stationary_Combustion.pdf

[30] Pöyry Management Consulting Oy, Suomen sähkötehon riittävyys ja kapasiteettirakenteen kehitys vuoteen 2030 (Capacity adequacy and the

future development of generation capacity until 2030 in Finland), Tech. rep., Pöyry Management Consulting Oy, Vantaa (2015).

[31] European Commission, Excise Duty on Energy (2003).
Available at: https://ec.europa.eu/taxation_customs/business/excise-duties-alcohol-tobacco-energy/excise-duties-energy_en

[32] P. Andreasen, T. Toivonen, O. H. Hoelsaeter, J. Magnusson, AGREEMENT (Translation) regarding operation of the interconnected Nordic power system (System Operation Agreement), Tech. Rep. 13, European Network of Transmission System Operators for Electricity (ENTSO-E), Stockholm (2006).

[33] UCTE Secretariat, OH Team, Continental Europe Operation Handbook (2004).
Available at: https://www.entsoe.eu/publications/system-operations-reports/#continental-europe-operation-handbook

[34] ENTSO-E, ENTSO-E Transparency Platform (2018).
Available at: https://transparency.entsoe.eu

[35] O. Wolfgang, A. Haugstad, B. Mo, A. Gjelsvik, I. Wangensteen, G. Doorman, Hydro reservoir handling in Norway before and after deregulation, Energy 34 (10) (2009) 1642–1651.
Available at: http://www.sciencedirect.com/science/article/B6V2S-4X1R2RK-2/2/fecd77eed29794b5b17299691ec3fbdc

[36] Finnish Environmental Administration, Hydrology and water resources information system HYDRO (2018).
Available at: https://wwwp2.ymparisto.fi/scripts/hearts/welcome.asp

[37] Copernicus Climate Change Service (C3S), ERA5: Fifth generation of ECMWF atmospheric reanalyses of the global climate. Copernicus Climate Change Service Climate Data Store (CDS) (2019).
Available at: https://cds.climate.copernicus.eu/cdsapp

[38] European Centre for Medium-Range Weather Forecasts (ECMWF), Set III - Atmospheric model Ensemble 15-day forecast (ENS) (2018).
Available at: https://www.ecmwf.int/en/forecasts/datasets/set-iii

[39] Portland State Aerospace Society, A Quick Derivation relating altitude to air pressure, Tech. rep., Portland State Aerospace Society (Dec. 2004). Available at: https://web.archive.org/web/20110928003908/http://psas.pdx.edu/RocketScience/PressureAltitude_Derived.pdf

[40] P. Nørgaard, H. Holttinen, A Multi-Turbine Power Curve Approach, in: Proceedings of the Nordic Wind Power Conference NWPC'04, Gothenburg, 2004.

[41] S. Pfenninger, I. Staffell, Long-term patterns of European PV output using 30 years of validated hourly reanalysis and satellite data, Energy 114 (2016) 1251–1265. doi:10.1016/j.energy.2016.08.060.

[42] The Wind Power, Wind Farms database, version 2017-12-07 (2017). Available at: https://www.thewindpower.net/index.php

[43] Open Power System Data, Data Package: Renewable power plants (2018).
Available at: https://open-power-system-data.org/

[44] D. Servén, C. Brummitt, H. Abedi, pyGAM: Generalized Additive Models in Python (2018). doi:10.5281/zenodo.1476122.
Available at: https://zenodo.org/record/1476122#.XOfBnmNRVaQ

[45] J. Kiviluoma, E. Rinne, T. Rasku, N. Helistö, Backbone - An adaptable energy system model (2018).
Available at: https://gitlab.vtt.fi/backbone/backbone

[46] IEC, IEC 61400-12-1 Power performance measurements of electricity producing wind turbines, Tech. rep., IEC (2017).

[47] I. Staffell, S. Pfenninger, Using bias-corrected reanalysis to simulate current and future wind power output, Energy 114 (2016) 1224–1239. doi:10.1016/j.energy.2016.08.068.
Available at: http://linkinghub.elsevier.com/retrieve/pii/S0360544216311811